Green hydrophilic capsules from CNC-stabilized Pickering emulsion polymerization: morphology control and sponge-like behavior

Hanaé Dupont, Eric Laurichesse, Valérie Héroguez, Véronique Schmitt

▶ **To cite this version:**

Hanaé Dupont, Eric Laurichesse, Valérie Héroguez, Véronique Schmitt. Green hydrophilic capsules from CNC-stabilized Pickering emulsion polymerization: morphology control and sponge-like behavior. Biomacromolecules, 2021, 22 (8), pp.3497-3509. 10.1021/acs.biomac.1c00581 . hal-03290989

HAL Id: hal-03290989
https://hal.science/hal-03290989

Submitted on 19 Jul 2021

HAL is a multi-disciplinary open access archive for the deposit and dissemination of scientific research documents, whether they are published or not. The documents may come from teaching and research institutions in France or abroad, or from public or private research centers.

L'archive ouverte pluridisciplinaire **HAL**, est destinée au dépôt et à la diffusion de documents scientifiques de niveau recherche, publiés ou non, émanant des établissements d'enseignement et de recherche français ou étrangers, des laboratoires publics ou privés.

Green hydrophilic capsules from CNC-stabilized Pickering emulsion polymerization: morphology control and sponge-like behavior

Hanaé Dupont[1,2], Eric Laurichesse[1], Valérie Héroguez[2,*], Véronique Schmitt[1,*]

[1] Centre de Recherche Paul Pascal, UMR 5031 Univ. Bordeaux CNRS, 115 avenue du Dr Albert Schweitzer, 33600 Pessac, France.

[2] Laboratoire de Chimie des Polymères Organiques, Univ. Bordeaux, CNRS, Bordeaux INP, UMR 5629, Bordeaux, 16 Avenue Pey-Berland, F-33607 Pessac, France.

* corresponding authors

veronique.schmitt@crpp.cnrs.fr

heroguez@enscbp.fr

Abstract

Pickering inverse emulsions of hydroxyl oligoethylene glycol methacrylate were stabilized in isopropyl myristate, a bio-friendly oil, using surface-modified cellulose nanocrystals (CNCs) as stabilizing particles. The emulsions were further polymerized by whether free or controlled radical polymerization (ATRP) taking advantage of the bromoisobutyrate functions grafted on the CNC surface. Suspension polymerization of the emulsion led to full beads or empty capsules morphologies depending on the initiation locus. Thickness of the CNC shell surrounding the polymerized emulsions could be tuned by modulating the aggregation state of the CNCs after their surface modification. An increase from 6 to 40 CNC layers helped improve the compression moduli of the beads from a dozen to hundreds of kPa.

Keywords

Cellulose nanocrystals, Pickering emulsion, ATRP, morphology, beads, capsules.

1. Introduction

Pickering emulsions, originally discovered in the beginning of the 20th century[1,2] regained interest in the early 2000's because of their high kinetic stability and their ease of implementation[3,4]. The use of particles also enabled the substitution of molecular scale surfactants, which are often deleterious regarding environmental and health concerns. For the particle choice, organic particles with natural origin have gained increasing interest over their inorganic and synthetic counterparts, because they appear as an economic and sustainable solution suitable for bio-related application, for instance[5]. From this perspective, cellulose nanocrystals (CNCs) constitute an interesting brick material: they are biosourced, biodegradable, with a well-known structure, they offer an easily modifiable surface and possess interesting intrinsic mechanical properties (Young modulus of 150 GPa)[6]. It has been shown that CNCs could be used for the stabilization of Pickering emulsions[7], and the polymerization of these emulsions was subsequently studied to produce polymer particles[8–11]. The stabilization and polymerization of CNC-stabilized oil-in-water (O/W) Pickering emulsions have been extensively studied, and both free and controlled radical polymerization[8,12–19] were considered. In previous contributions of our group, Werner *et al.* showed that the resulting polymer particle morphology could be tuned by varying the polymerization process and conversion[8,20]. It was demonstrated that by using ATRP initiated at the stabilizing CNC surface and by targeting low conversion rates, hollow beads could be obtained, whereas full beads were obtained for high monomer conversions or by using free radical polymerization. On the contrary, very little literature have been dedicated to the polymerization of water-in-oil (W/O) Pickering emulsions stabilized by organic particles with natural origin[5,21,22], and even less considered the use of cellulose nanocrystals or cellulose derivatives[10]. Among them, free radical polymerization was systematically studied, and the sole impact on the morphology reported used poly(N-isopropylacrylamide) and its loss of solubility in water at high temperatures to produce hollow microcapsules[10]. To our knowledge, no reference of controlled radical polymerization of water-soluble monomers within Pickering emulsions stabilized by natural organic particles, and in particular CNCs, has

been reported so far. Therefore, herein we chose to investigate the formulation and polymerization of CNC-stabilized W/O Pickering emulsions, using both free and controlled radical polymerizations of hydroxyl oligoethylene glycol methacrylate. In the present work, we propose to study the impact of the polymerization route on the polymer particle morphology, as well as the reinforcement induced by the presence of the CNC shell covering these polymer particles (Figure 1).

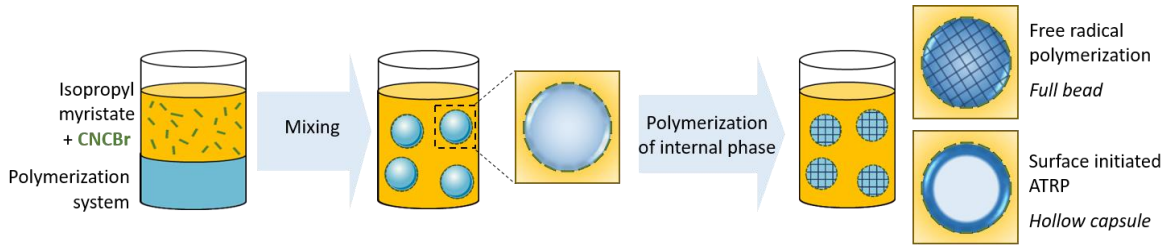

Figure 1: Principle scheme for the formulation and synthesis of the polymer particles.

2. Experimental

2.1 Materials

Pristine CNCs used in this study were purchased from The University of Maine, under freeze-dried CNC form, isolated from sulfuric acid hydrolysis of wood pulp. The crystals present initially on their surface both sulfate (1.05 wt% as data from the provider) and hydroxyl functions (3.10 ± 0.11 mmol.g^{-1} of CNC). The initial CNCs presented rod-like shape with estimated dimension of L=138 ± 47 nm in length and l=25 ± 6 nm in width based on AFM analysis (Fig. S1, SI).

Triethylamine (TEA) (Fisher scientific, 99%), α-bromoisobutyryl bromide (Bibb) (ABCR, 98%), dimethylaminopyridine (DMAP) (Sigma Aldrich, 99%) were used for the CNC modification without any purification. Isopropyl myristate (IPM) (98%, Alfa Aesar), an oil allowed for cosmetic applications, was used as received as oil phase for all the inverted emulsion systems. Hydroxyl oligoethylene glycol methacrylate (OEGMA, M_n = 360 g/mol) (Sigma Aldrich) and tetraethylene glycol diacrylate (TEGDA) (Sigma Aldrich) were used as macromonomer and cross-linker without purification. Potassium persulfate (KPS) (>99%, Sigma Aldrich), copper(II) bromide ($CuBr_2$) (99%, ABCR), tris(2-pyridylmethyl)amine (TPMA)

(98%, Sigma Aldrich), 2-hydroxyethyl 2-bromoisobutyrate (HOEbib) (95%, Sigma Aldrich), ascorbic acid (AA) (99%, Acros) were used as received.

2.2 CNC-Br synthesis

CNC-Br synthesis was first described by Zhang *et al.*[23] and Morandi *et al.*[24], modified by Werner *et al.*[8] and optimized in the present work. 2 g of CNC and 2 g of DMAP were introduced in a double wall reactor. After a nitrogen purge, 100 mL of dry DMF were added to the powders under gentle agitation with a magnetic stirrer. The solution was cooled down to 0°C. 8.5 g (1.48 mol/L) of Bibb (reactant) and 4.8 g (1.90 mol/L) of TEA, were added to the solution under vigorous agitation. After 14.5 h or 41 h, CNC-Br were precipitated in 200 mL of a mixture of THF/ethanol ($50/50_{v/v}$), isolated by centrifugation (6000 rpm, 10 min, 15°C) and redispersed in water. THF was subsequently added to the CNC-Br dispersion before centrifugation. This step was repeated at least 3 times to remove all unreacted species. The final dispersion in water was freeze-dried to obtain a white powder.

The grafting was confirmed by CP MAS NMR and FT-IR by following the apparition of the stretching bonds corresponding to the surface ester group at 1760 cm^{-1} (ν(C=O)) and 1060 cm^{-1} (ν(C-O)) (Fig. S1, SI). Quantitative evaluation of modification rates was determined by elemental analysis thanks to the mass percentage of bromine and the amount of surface hydroxyl groups (Eq. 1).

$$\%\ substitution = \frac{mmol\ of\ Br\ by\ gram\ of\ CNCs}{mmol\ of\ surface\ hydroxyl\ functions\ by\ gram\ of\ CNCs} = \frac{n_{Br}}{n_{OH}}.100 \qquad \textit{Eq. 1}$$

with n_{OH} = 3.10 $mmol.g^{-1}$.

2.3 Formulation and characterization of Pickering emulsions

2.3.1 Pickering emulsions for Free radical polymerization

The organic continuous phase was composed of 3 ml of IPM and CNC-Br (ranging from 10 to 50 g/L of dispersed phase). The nanoparticles were dispersed as best in IPM using an ultrasonic bath. The aqueous phase was composed of the polymerization system containing a macromonomer OEGMA (concentration ranging from 10 to 40 wt%), possibly a cross-linker TEGDA (15 mol% compared to the total amount of macromonomer) diluted in salted water

(NaCl, 40 mmol/L) and the free radical initiator KPS (1 g/100 g (macro)monomer(s)). The two phases were mixed in $25/75_{v/v}$ ratio for a total volume of 4 ml using a rotor-stator, Ultraturrax® S18N-10G, at 15 000 rpm during 30 seconds to obtain water-in-oil emulsions. A control emulsion was also formulated without any CNC-Br, but no stable emulsion was obtained.

2.3.2 Pickering emulsions for Surface-Initiated controlled radical polymerization (SI-ATRP)

The same organic phase as previously described was used. The aqueous phase was composed of two distinct solutions: the first one containing the macromonomer, and the catalytic system composed of a metal $CuBr_2$, a ligand TPMA, and a sacrificial initiator HOEbib ([macromonomer]/[$CuBr_2$]/[TPMA]/[HOEBib] = 200/0.5/0.5/1). The second solution contained the reducing agent AA (1000 mol% compared to the $CuBr_2$ content). All three solutions were purged with nitrogen for 30 min, then the two aqueous phases were mixed before being added to the organic phase. Emulsification was performed right after, using a rotor-stator, Ultraturrax®, S18N-10G, at 15 000 rpm during 30 seconds to obtain a water-in-oil emulsion. The vial containing the emulsion was sealed and nitrogen-purged IPM (approximately 6 ml) was subsequently added to fill the whole vial headspace prior to polymerization.

For both polymerization systems, particle size distribution was obtained by measuring the diameter of a hundred droplets using ImageJ software processing on optical microscopy images. The surface average diameter, or Sauter diameter $D_{3,2}$ was calculated following the equation:

$$D_{3,2} = \frac{\sum_i N_i D_i^3}{\sum_i N_i D_i^2} \qquad \textit{Eq. 2}$$

Where N_i is the number of droplets with diameter D_i. Standard deviation were accordingly measured for each droplet size distribution.

2.4 Polymerization of Pickering emulsions

2.4.1 Pickering emulsions polymerized by Free radical polymerization

The emulsions were placed in an oil bath at 75°C for 24 h. To perform conversion kinetics measurements, polymerization was stopped at different times by exposure to air. The obtained polymer particles were washed with ethanol and the supernatant containing unreacted (macro)monomer(s) and IPM was removed. This step was operated at least three times to ensure removal of all residual (macro)monomer(s) and solvent. Conversions were obtained by gravimetric measurements.

2.4.2 Pickering emulsions polymerized by SI-ATRP

The emulsions were placed on a rotating stirrer wheel at 6 rpm inside an oven at 50°C for 2 h. To follow the polymerization kinetics, aliquots of the emulsions were withdrawn periodically and replaced by nitrogen-purged IPM to ensure a constant volume. The aliquots were dispersed into deuterated THF (THF-d8) using a vortex and an ultrasonic bath. Conversion were obtained by ^{1}H NMR from integration of the macromonomer vinyl protons (a, b, δ = 5.5 - 6 ppm, Fig. S2, SI) and the PEG pending-chain protons (e-g, δ = 3.5 ppm, Fig. S2, SI).

2.5 Instrumentation

Infrared spectra of unmodified and brominated CNCs were recorded using a Vertex 70 Bruker FT-IR spectrometer. CNC powder was analyzed thanks to an attenuated total reflectance ATR accessory. Each spectrum was recorded between 4000 cm^{-1} and 400 cm^{-1} with a resolution of 4 cm^{-1} with 32 scans.

Optical micrographs were taken on a bright-field upright microscope (Zeiss Axioscope 40) and the recorded images were analyzed with ImageJ.

Scanning electron microscopy (SEM) observations were performed with a HITACHI TM-1000 apparatus operating at 15 kV. Samples were coated with a layer of Au-Pd before observation using a plasma at 10 mA for 30 s.

Contact angles were measured on a Teclis apparatus using the drop deposit technique. Pellets of CNCs were produced from 200 mg of CNC-Br using a 13 mm Evacuable Pellet Die and a manual hydraulic press (5 tons during 1 min). The pellets were kept dry in an oven at 50 °C prior to experiment. Drops of salted water containing various concentration of

macromonomer (4 µL) were deposited on the pellets and the contact angle was measured. For each macromonomer concentration, the contact angle was measured at least two to three times.

Interfacial tension was measured on a Teclis apparatus using the pendant drop technique. An aqueous drop of salted water containing various concentration of macromonomer (4 µL) was immersed into IPM during 2000 s, and the tension was recorded as a function of time. The tension was calculated from the axisymmetric drop shape by fitting with the Laplace equation.

NMR spectra were recorded on a Bruker Avance 400 (^{1}H at 400.2 MHz) in deuterated THF (THF-d8) solvent with t_{relax} = 1 s and n_{scan} = 16.

The polymer particles were analyzed by Thermogravimetric Analysis (TGA) using a Q500 device from TA Instruments with a ramp of temperature from 25 °C up to 600 °C with a speed of 10 °C/min under N_2 atmosphere. The polymer particles were further analyzed by Differential Scanning Calorimetry (DSC) using a DSC Q100 RCS device from TA instruments. Two heating runs were performed. During the first cycle, an increase of temperature from -80 °C to 120 °C with a speed of 10 °C/min followed by a decrease down to -80 °C was programmed. The second cycle started at -80 °C up to 230 °C with a speed of 10 °C/min followed by a last decrease down to -50 °C at the same speed.

Compression tests were performed using a rheometer (AR2000, TA Instruments) equipped with a plate-plate geometry of 40 mm in diameter. Dispersion of polymer particles in IPM (8 ml total volume, water to oil ratio 25/75$_{v/v}$) was put into a homemade device adapted from previous work[25], constituted of an empty cup, in which a hollow piston is pressed with a stainless-steel filter of 5 µm pore size, without the rubber joint. The top plate of the rheometer was lowered at 1 µm/s pushing the hollow piston and therefore compressing the polymer beads contained in the cup, letting the IPM be expelled through the filter. The normal stress was measured. The compression step was followed by a Peak-hold step of 60 seconds for which the strain was maintained. Afterwards, the top plate of the rheometer was elevated at 1 µm/s and the normal stress was measured to evaluate the sample relaxation. Compression

modulus was extracted from the slope of the linear elastic domain of the stress-strain curve. Compression tests were repeated at least 3 times to ensure a representative average compression modulus value. Compression tests were also performed using a traction force apparatus (Zwick/Roell Amsler Z2.5) equipped with a force sensor of 100 N.

3. Results and discussion

3.1 CNC modification

3.1.1 Impact of CNC-Br substitution rate on Pickering emulsion stability

Pristine cellulose nanocrystals obtained from wood pulp after acid hydrolysis bear on their surface mainly hydroxyl functions giving them a highly hydrophilic nature. Modification of the surface functions was broadly studied, and in previous works, we showed that esterified CNCs were able to stabilize efficiently both direct and inverted Pickering emulsions[8,26]. Thus, the esterification of CNC by Bibb was used in the present study in order to modify the nanoparticles hydrophobic/hydrophilic balance, in a fast and easy way. IPM is a polar oil and therefore less hydrophobic than usual alkanes generally used to stabilize Pickering emulsions[10,27,28]. The dispersion of the mainly hydrophobic CNC-Br in IPM was thus limited because of the lack of affinity between the solvent and the nanoparticles, and a particular attention was put on the modification rate of the CNC-Br. Contrary to previous studies where a substitution rate of 100% was satisfactory, here a specific modification rate was targeted to induce specific hydrophobic/hydrophilic balance and therefore efficient stabilization of inverted emulsions. The optimum modification rate was targeted over 50% to ensure enough hydrophobicity, and observation of emulsion stability narrowed it around 80%, as higher modification rates (100%) lead to poor CNC adsorption and therefore poor emulsion stability (Figure 2). If the CNCs are too hydrophobic as it is the case for 100% modification rate, a large proportion of CNCs remain dispersed in oil and are inefficient for emulsion stabilization leading to a fast destabilization (Figure 2b).

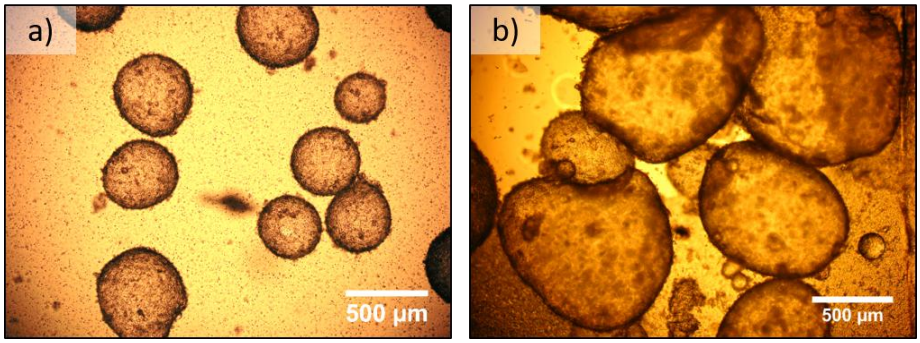

Figure 2: Pickering emulsion stabilized with CNC-Br modified at a) about 80% and at b)100%.

3.1.2 Impact of the washing step over the aggregation of the modified CNC-Br

It has also been observed that the way the washing is performed prior to freeze drying, is of great importance towards the final hydrophobically modified CNC-Br redispersion in a hydrophobic polar medium. Indeed, the washing comprises a dispersion step of CNC-Br in a water/THF mixture. The order of introducing water and THF matters. When water was primarily used to redisperse the CNC-Br and THF was added afterwards, the CNCs tended to aggregate due to the very poor affinity with water. This phenomenon was hardly reversible since CNC-Br obtained after freeze-drying showed important aggregates size. On the contrary, when THF was primarily used, CNC-Br were better dispersed before being put in contact with a poor solvent (water). This second procedure allowed achieving better and easier redispersion of CNC-Br in a polar medium such as IPM. Therefore, stabilizing particles are more available during the emulsion formulation leading to a decrease of the droplet mean diameter and also a decrease in the covering ratio of the droplets (proportion of droplets interfacial area covered by the CNC, a more detailed definition and the way it is measured are given by Eq. 4) (Figure 3, Fig. S3, SI). This constitutes an interesting parameter to control, as the covering ratio might influence the mechanical properties of the final objects, as we will see later.

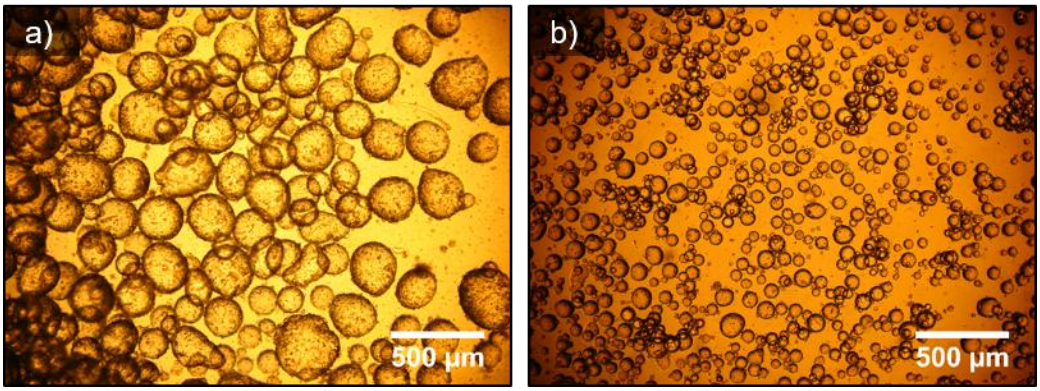

	Emulsion a)	Emulsion b)
CNC batch n°	CNC-Br 2A	CNC-Br 2B
Concentration of CNC (g/L of dispersed phase)	18	18
$D_{3,2}$ (µm)	209 ± 54	74 ± 16
Coverage	16	6

Figure 3: Pickering emulsions stabilized by CNC-Br issued from the same modification batch with different washing procedures (Fig. S3, SI); all emulsions were obtained using the same formulation and process, with IPM as continuous phase. a) water was used as first redispersing solvent during the washing step; b) THF was used as first redispersing solvent.

In the following, unless otherwise specified, CNC-Br washed first by water and then by THF were used. Their main characteristics are specified in Table 1. Indeed, using highly aggregated CNC-Br, which lead to emulsion droplets with a high covering ratio, might be of interest to exacerbate the potential improvement in the mechanical properties induced by the presence of the CNCs.

Modification features	CNC-Br 1
Duration of the reaction (h)	41
$\%_{wt}$ of Br	21.98
mmol of Br per gram of CNC	2.75
Substitution rate (%)	89

Table 1: Substitution rate of CNC-Br from Br-elemental analysis

3.2. Formulation and Free radical polymerization of Pickering emulsions

3.2.1 Pickering Emulsions formulation

IPM, which is a non-toxic oil widely used in cosmetics and pharmaceutics was chosen as continuous phase for all emulsions formulated in this study. For the same purposes, functionalized PEG was chosen as macromonomer (OEGMA) and cross-linker (TEGDA) to obtain at the end an overall bio-friendly system stabilized by CNCs.

In the first place, emulsion optimal formulation parameters were determined. The volume fraction of dispersed phase was set to 25 %v to work in diluted conditions favoring the formation of inverse emulsion. Moreover, higher volume fraction of dispersed phase directly emulsified ended up in the destabilization of the emulsion. The macromonomer concentration was varied, ranging from 10 wt% to 80 wt% with respect to the dispersed phase (Figure 4A). Stable emulsions could only be formulated with an OEGMA concentration lower or equal to 40 wt%, most probably because of the important affinity between the macromonomer and the modified CNCs, as it was verified by contact angle measurements (Figure 4B, C). The increase in macromonomer fraction within the aqueous phase increases the contact angle of the adsorbed CNCs at the interface. This experiment also shows that the concentration of OEGMA within the aqueous phase affects the adsorption properties of the CNCs at the interface. Indeed, the desorption energy for parallelepiped rods can be calculated as[29]:

$$\mathrm{E}_{\mathrm{desorption,rod}} = \gamma_{\mathrm{o/w}}\mathrm{A}(1 - |\cos\theta|) \qquad \textit{Eq. 3}$$

with $\gamma_{o/w}$ the interfacial tension between IPM and the water phase, A the surface covered by one CNC at the interface (A=Lxl), and θ the contact angle.

The desorption energy varies with the contact angle, when θ decreases the desorption energy becomes very low (Figure 4C). Therefore, a high OEGMA content in the aqueous phase induces the emulsion destabilization, because of the poor adsorption of the CNCs at the interface. It is worth noting that the desorption energy also depends on the interfacial tension $\gamma_{o/w}$ between IPM and the water phase, which decreases with increasing OEGMA content (Figure 4D). Hence both parameters contribute to the decrease of the desorption energy with increasing OEGMA content, which explain the destabilization of emulsions containing high amounts of macromonomer within the aqueous phase.

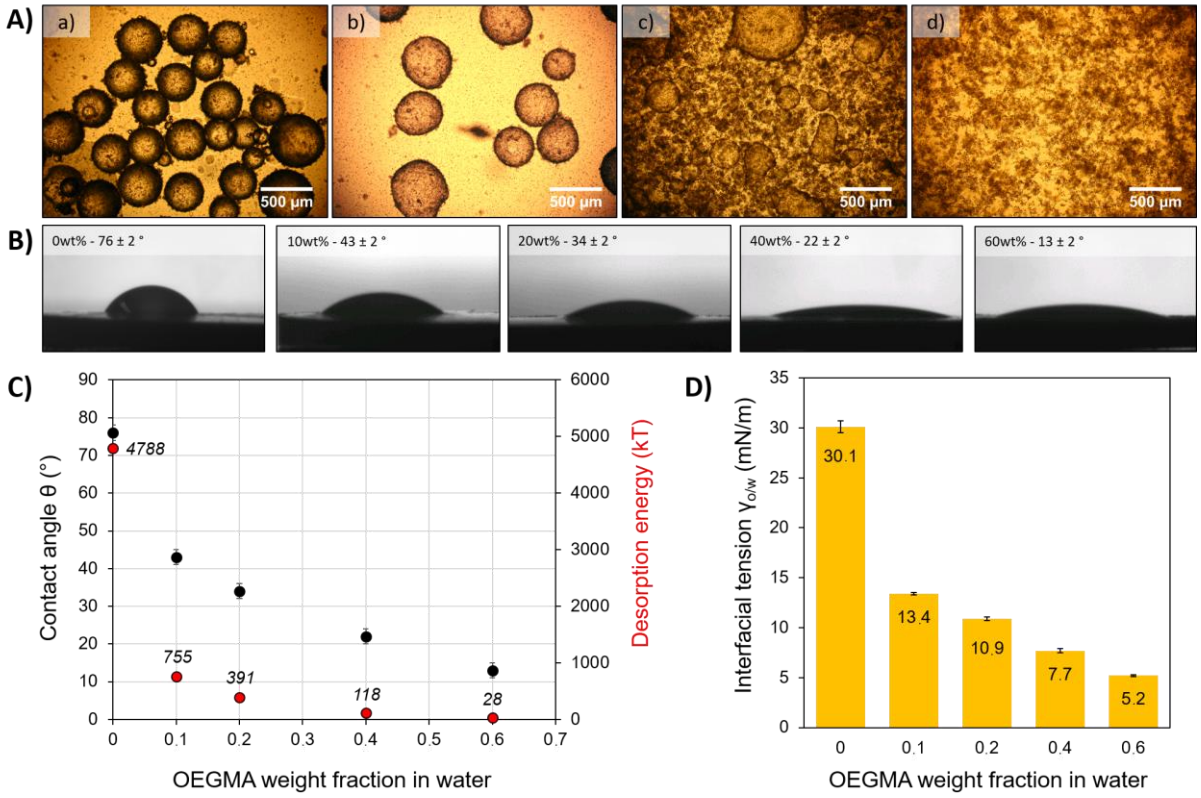

Figure 4: A) Observation by optical microscopy of the inverted emulsions containing OEGMA at different concentrations a) 10 wt%, b) 40 wt%, c) 60 wt%, d) 80 wt%, B) Contact angle measurement between CNC-Br pellets and aqueous solutions with various macromonomer concentrations, and C) respective desorption energy with D) according interfacial tension.

A cross-linker was eventually added in the polymerization system to evaluate its impact on the final properties. Its maximum concentration was similarly assessed and finally its content was set to 15 mol% with respect to the total (macro)monomers concentration (equivalent to 5 wt% with respect to the aqueous phase), higher cross-linker molar ratio leading to emulsion destabilization (films of broken emulsion droplets can be seen in Fig. S4, SI). It is worth noticing also that for a fixed (macro)monomer concentration and at a given CNC concentration, the addition of the cross-linker didn't change the emulsion diameter, within error. Indeed, $D_{3,2}$ is equal to 584 ± 176 µm without cross-linker and 542 ± 113 µm in presence of TEGDA.

Stable emulsions were successfully obtained using CNC as stabilizing particles with concentrations varying from 10 to 40 g/L of dispersed phase. The Sauter diameter $D_{3,2}$ was measured and its inverse was plotted against the CNC concentration (Figure 5) showing a linear dependence. This observation is consistent with the limited coalescence phenomenon

characteristic of Pickering emulsions in the particle-poor domain given the irreversible adsorption of stabilizing particles at the interface[30,31]. In these conditions, it is possible to extract from the slope the covering ratio, C, defined as the proportion of interface covered by the particles, thanks to the following equation[32]:

$$\frac{1}{D_{3,2}} = \frac{m_p}{6\rho_p V_d C} \cdot \frac{a_p}{v_p} \qquad \textit{Eq. 4}$$

where m_p corresponds to the mass of particles, ρ_p their density (taken as 1.6 g/cm^3), a_p and v_p the projected surface and the volume of the particles in contact with the interface (140x25 nm² and 140x25x25 nm^3 respectively, approximating the CNC shape to a parallelepiped rectangle), V_d the volume of the dispersed phase, and C the covering ratio. For parallelepiped particles as CNC, a C value of 1 corresponds to a dense monolayer. If C>1, then the droplets are covered in average by multilayers of CNC following C = n x 100 %. For the present system C ≈ 41, which means in average, 41 layers of CNC are attached to the droplets surface likely as the result of CNC aggregates that stabilize the emulsions. Aggregates are due to the washing procedure and the quality of the first used solvent (See section 3.1.2). The large amount of CNC on the surface is even visible by optical and electronic microscopy showing a rough solid interface (Figure 5, Figure 13). The deformation of the emulsion droplets also assesses for the rigidity of the interface. Indeed, coalescence phenomena occurring between droplets usually lead to shape relaxation to obtain a spherical droplet. However, the more rigid the interface, the more difficult the shape relaxation and as a result the more deformed the drops. This is the case depicted in Figure 5. As proposed earlier (see section 3.1.2), the CNC aggregation in the dispersed media is also due to the oil choice, additionally to the washing procedure prior to freeze-drying. Indeed, originally aggregated CNCs because of the washing procedure can be more or less redispersed for the emulsion formulation depending on the oil choice. Hence, using IPM which is a polar oil, and therefore a poor solvent for the CNCs, will not help in a good redispersion of the nanocrystals. In opposition by replacing IPM by a non-polar hydrophobic oil like toluene, which is a better solvent for CNCs redispersion, and keeping all other parameters constant,

the CNCs are better dispersed and a C parameter of 8 can be reached leading to smaller droplet diameters (Fig. S5, SI).

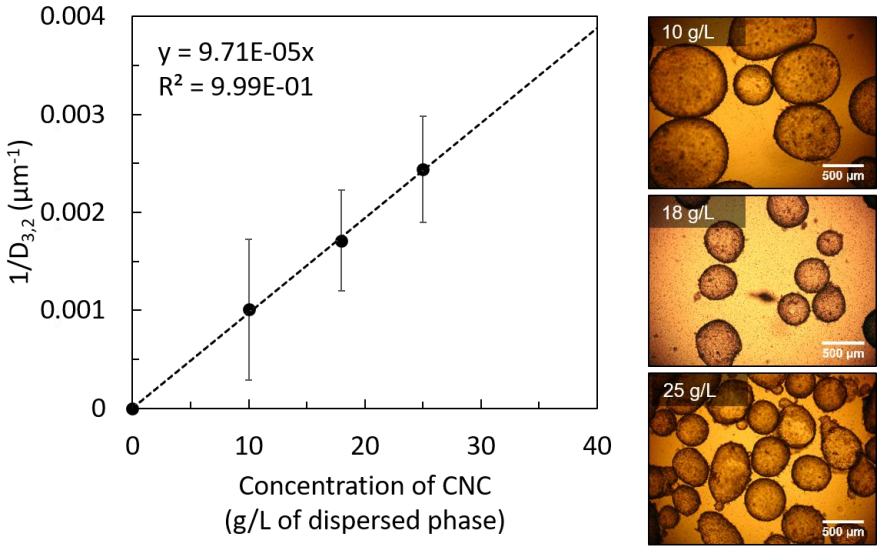

Figure 5: Left, Reverse drop diameter as a function of the amount of CNC-Br in the organic phase for the free radical polymerization system. All the other parameters are kept constant: 25/75v/v of aqueous phase/IPM, OEGMA 40 wt% no TEGDA. The linear variation highlights the limited coalescence phenomenon occurring in this concentration range. The error bars reflect the drops size distribution width. Right, optical microscopy observation of corresponding emulsions. From the slope of the curve the coverage rate of 41 can be estimated.

3.2.2 Pickering Emulsion polymerization

For the following, the CNC concentration was fixed at 18 g/L with respect to the dispersed phase to formulate all the emulsions in the limited coalescence domain. The emulsions formulated with the macromonomer alone and with both macromonomer and cross-linker (10 wt%, 40 wt% in (macro)monomer(s) with respect to the aqueous phase) were polymerized by heating the samples for 24 h in a 75 °C oil bath. The emulsions were stable upon heating and upon (macro)monomer(s) conversion. No coagulate was formed during the polymerization process and the obtained polymerized emulsions were redispersible in the continuous IPM phase. Droplet size and drop size distribution width were conserved within error through polymerization as verified by optical microscopy (*Figure 6*): for the emulsion with 40 wt% OEGMA, indeed the emulsion drop size before polymerization was 584 ± 176 µm and after polymerization 472 ± 114 µm. Interestingly, in previous studies performed by our group for similar polymerization systems within emulsions stabilized by surfactants, the obtained OEGMA/TEGDA latexes were only redispersible in aqueous medium, and not in the

polymerization medium IPM, given the high hydrophilicity of the OEGMA/TEGDA polymer[25]. In the present case, the polymerized emulsions are only redispersible in organic media, likely due to the hydrophobic shell constituted by the brominated CNCs irreversibly adsorbed at their interface masking the hydrophilic polymer behavior.

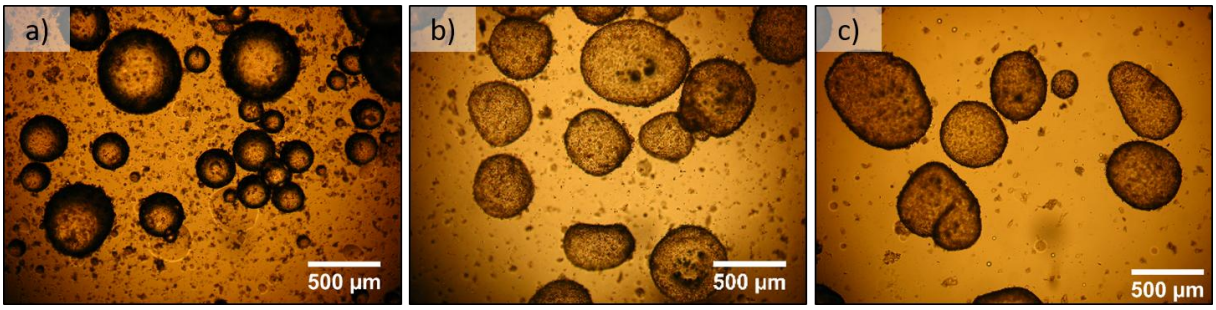

Figure 6: Optical microscopic observation of the emulsions after polymerization for different concentrations of macromonomer and cross-linker (OEGMA, TEGDA) a) (10 wt%, 0) b) (40 wt%, 0) and c) (35 wt%, 5 wt%)

The polymerization conversion was followed by gravimetric measurement over 24 h for different OEGMA concentrations and in presence of TEGDA. All formulations reached high conversions of a minimum of 70% (Figure 7). Maximum conversion was achieved in most cases in 6 h. The final overall conversion (OEGMA and TEGDA) is higher with increasing macromonomer content. Indeed, as the emulsion droplets act as small reactor vessels, the encounter of macromonomers with reactive sites is strongly limited when the dilution increases. The increase in macromonomer concentration also increases the chain length, thus limiting the mobility of reactive sites and consequently secondary reactions like recombination or termination, and allows reaching higher conversion. However, this increase in viscosity is also a limiting parameter regarding the final conversion of the macromonomer which does not exceed 80% (Fig. S6, SI).

When adding TEGDA, copolymerization between acrylates and methacrylates monomers must be considered. Acrylates react faster than methacrylates because of the lower stability of secondary radicals in comparison with tertiary radicals[33]. Moreover, addition of acrylates, which are less sterically hindered helps in stimulating conversion, rendering active site more accessible to macromonomers, thus helping reaching higher conversion rates, up to 90%.

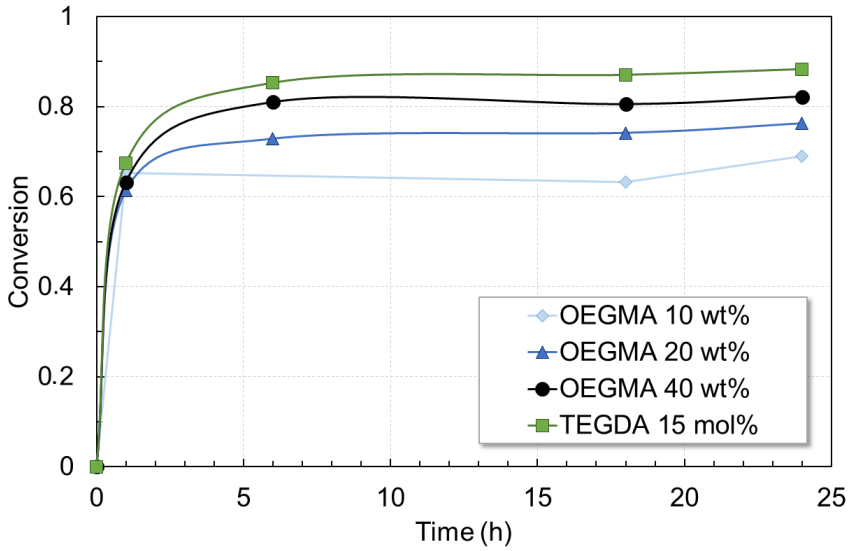

Figure 7: Conversion kinetics over time for different concentrations of OEGMA 10 wt%, 20 wt%, 40 wt%), and with the presence of TEGDA as cross-linker (35 wt% OEGMA, 5 wt% TEGDA).

The effect of the chemical cross-linking was assessed by thermal analyses (DSC and TGA) of the polymer particles (Figure 8, Fig. S7, SI). The DSC thermograms are consistent with the polyethylene glycol entities present within the OEGMA, with a glass transition temperature (T_g) around – 50 °C and a crystallization and fusion around respectively – 7 °C and 5 °C[34]. The loss of mobility of the pendant PEG chains with increasing cross-linker concentration caused the shift of the T_g towards higher temperature values, and the disappearance of the crystallization and fusion peaks[25,34]. This observation is consistent with TGA analyses which show also a shift of the polymer degradation temperature towards higher temperature values with addition of the cross-linker (from 350 °C to 400 °C). The presence of the chemical network induced by the cross-linking was also demonstrated by following the swelling behavior of gels obtained from polymerization of the polymeric system in solution (Fig. S8, SI). The gels containing TEGDA were unable to absorb as much water as its counterpart without TEGDA due to the limited volume expansion as a result of the presence of the cross-linking. Maximum swelling ratios of 400% and 200% were measured for OEGMA and OEGMA-co-TEGDA gels respectively.

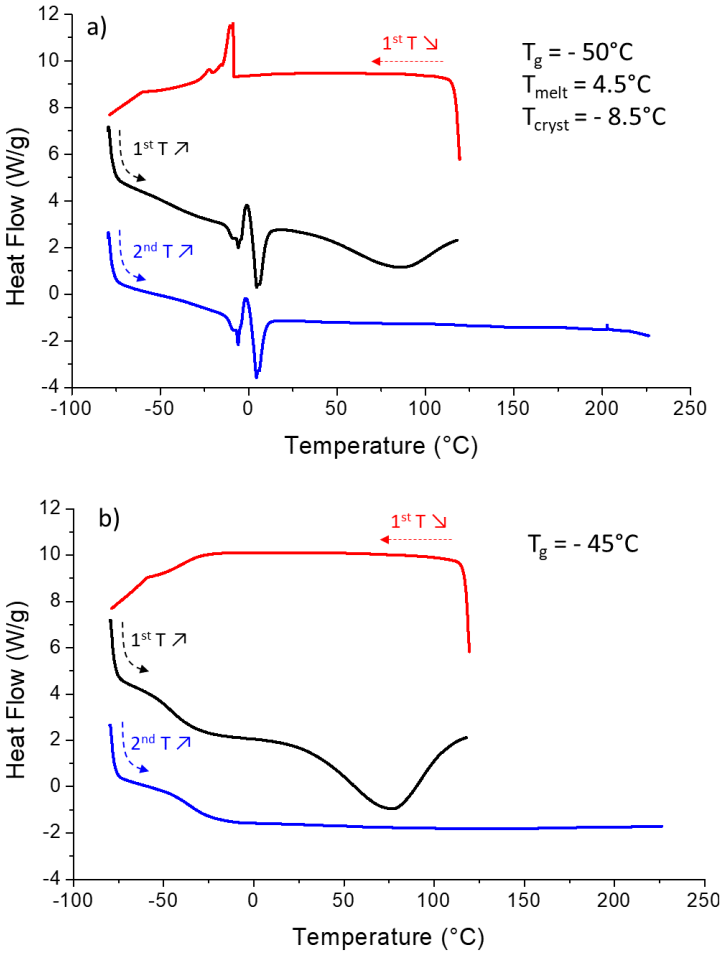

Figure 8: DSC thermograms of polymer particles a) without and b) with cross-linker

3.3. Formulation and SI-ATRP of Pickering emulsions

Another polymerization route was considered taking advantage of the surface modification performed on the CNC-Br. Pickering emulsions SI-ATRP was performed initiating the polymer growth from the brominated functions grafted on the CNC-Br, therefore linking covalently the polymer to the CNC-Br shell (Figure 9).

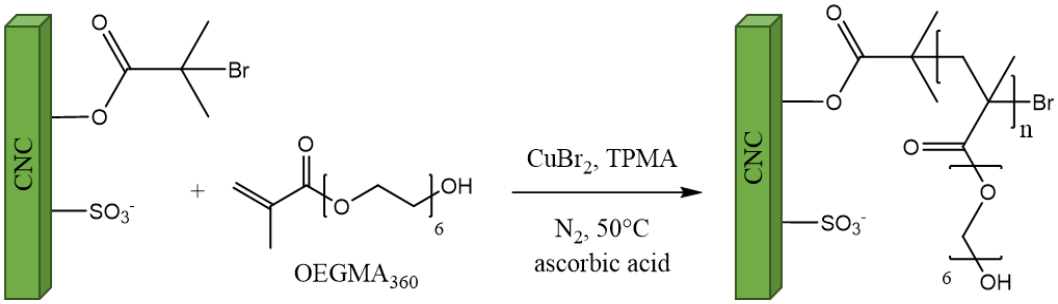

Figure 9: Reaction scheme of the SI-ATRP initiated at the CNC-Br surface.

3.3.1 Pickering Emulsion formulation

Formulation parameters determined in section 3.2.2 were kept constant for this new route. The W/O emulsion fraction was set to 25/75$_{v/v}$, the OEGMA concentration in the aqueous phase was set at 40 wt%. The polymerization of OEGMA was initiated from the CNC-Br surface. A water-soluble sacrificial initiator HOEBib was added in the medium to follow the conversion by ^{1}H NMR. The catalyst $CuBr_2$/TPMA was added to the aqueous phase and ascorbic acid used as a reducing agent to convert the Cu(II) in active Cu(I) complex.

As for the previous free radical polymerization system, the Sauter diameter $D_{3,2}$ of the obtained emulsions was measured and its inverse was plotted against the CNC-Br concentration (Figure 10).

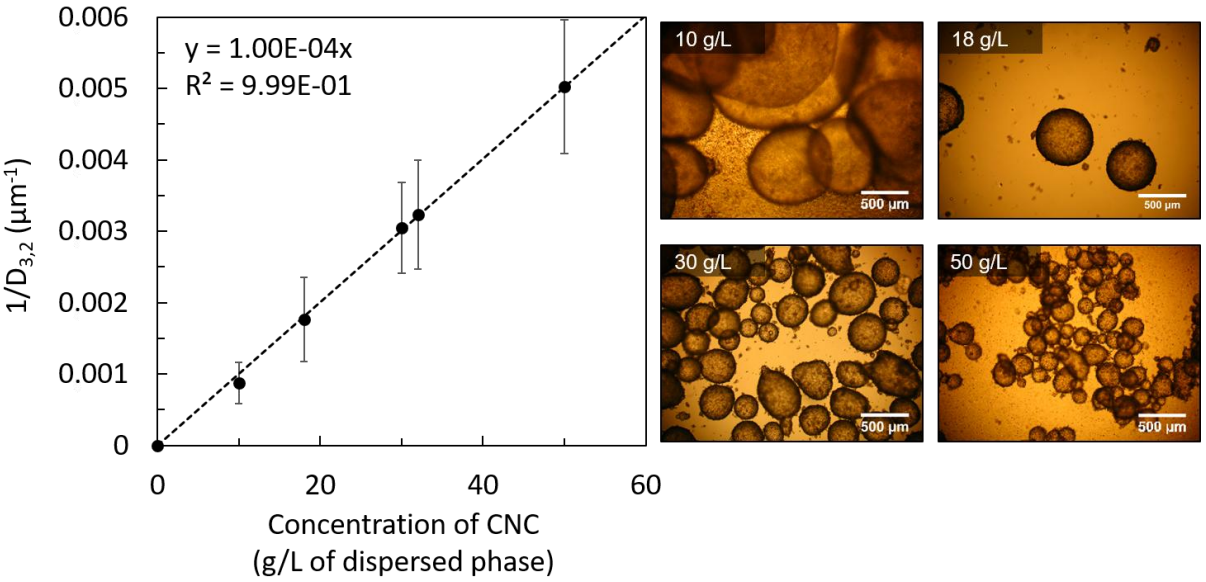

Figure 10: Left, Reverse drop diameter as a function of the amount of CNC-Br in the organic IPM phase for the SI-ATRP system. All the other parameters are kept constant: 25/75$_{v/v}$, OEGMA 40 wt%, [OEGMA]/[$CuBr_2$]/[TPMA]/[HOEBib] = 200/0.5/0.5/1. The linear variation highlights the limited coalescence phenomenon occurring in this concentration range. The error bars reflect the drops size distribution width. Right, optical microscopy observation of according emulsions.

What is noticeable from this plot is that the SI-ATRP system shows the exact same behavior from a colloidal point of view as the free radical polymerization system. The two graphics superimpose perfectly, which is due to the very similar composition of both organic and aqueous phase in the two polymerization routes (Fig. S9, SI).

3.3.2 Pickering Emulsion polymerization

Proportion of each component was optimized from Matyjaszewski and coll. work[35], by studying first the polymerization in aqueous solution. Following experimental conditions described in the literature[35], and after determination of optimal AA/$CuBr_2$ molar ratio (Fig. S10, SI) good conversion measured by ^{1}H NMR were obtained. Macromonomer conversion of 87% in 2 h was reached in solution using a ratio of [OEGMA]/[$CuBr_2$]/[TPMA]/[HOEBib] = 200/0.5/0.5/1, a molar ratio AA/$CuBr_2$ = 50 mol%, at ambient temperature (Fig. S10, SI). When transposing this set of parameters to the emulsion system, the conversion achieved in 2 h was only of 23% and emulsion droplets were aggregated (ATRP-1, Table 2). The gap between the monomer conversion in solution and in suspension can be explained by the change in the initiator availability in the emulsion system. Indeed, the initiating brominated functions are principally located at the droplet surface, which is small and the CNC-Br initiation efficiency is probably lower than its soluble alkyl halide counterpart's. Concerning the aggregation of the droplets during polymerization, several explanations can be proposed. The interfacial position of the initiation loci might have led to polymer chain interpenetration from neighbor emulsion droplets. This phenomenon could have been even more aggravated because of the rapid sedimentation of the emulsion droplets due to their important dimension (Fig. S11, SI). However, a change in the hydrophilic/lipophilic balance of the CNC with increasing polymer grafts can also be considered. This last hypothesis has already been proven right in a previous work[8]. Indeed, the polymerization of styrene by ATRP into O/W CNC-Br-stabilized emulsions induced the migration of the newly formed CNC-polySt-Br into the core of the droplet. This phenomenon could very well occur in our system, with a possible migration of the stabilizing CNC into the core, thus not present anymore at the interface to ensure the emulsion stabilization.

The reaction parameters were optimized to achieve both high conversion but also emulsion stability over polymerization (Table 2). Molar ratio of AA/$CuBr_2$ and temperature were increased to respectively 1000 mol% and 50°C, to obtain equivalent conversion as in solution with milder conditions (50 mol% AA/$CuBr_2$, ambient temperature, Fig. S12, SI). Regarding

aggregation, a rotating stirrer wheel was used to prevent permanent contacts between droplets while providing a gentle agitation.

ID	Conversion (%)	AA/$CuBr_2$ (mol%)	Temp (°C)	Agitation	Stability
ATRP-1	23	50	Amb.	None	Ag.
ATRP-2	58	100	Amb.	None	Ag.
ATRP-3	63	100	50	None	Ag.
ATRP-4	40	1000	Amb.	Wheel	Ok
ATRP-5	86	1000	50	Wheel	Ok

Table 2: Reaction parameters optimization to achieve higher conversion with emulsion stability; Amb.: ambient, Ag.: aggregated, Ok: well dispersed.

The conversion within the emulsion was followed by ^{1}H NMR (Figure 11). Because CNCs cannot undergo usual ^{1}H NMR analysis, the polymer-grafted CNCs were not directly analyzed. Instead, free polymer chains initiated by HOEBib sacrificial initiator were extracted from aliquots withdrawn from the emulsion and analyzed. In comparison with the free radical polymerization which achieved 80% conversion in 6 h, the optimized ATRP system reached similar conversions in less time (ATRP-5, over 80% in 2 h).

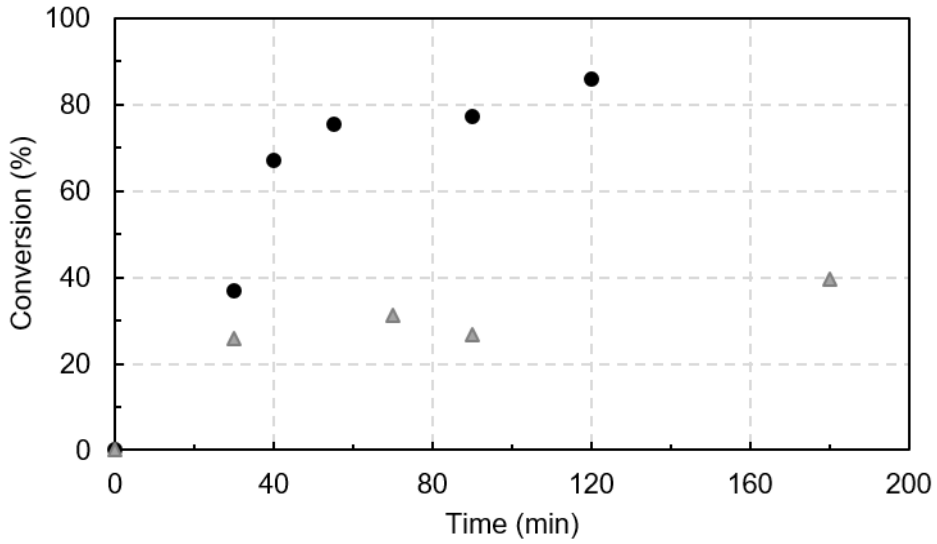

Figure 11: Conversion in emulsion with 1000 mol% AA/$CuBr_2$ at different temperatures: ATRP-4 at ambient temperature 25°C (grey triangle) and ATRP-5 at 50°C (black circle).

From a colloidal point of view, emulsions were stable upon heating and macromonomer conversion, thanks to the rotating stirrer wheel which prevented the formation of a coagulum (Figure 12). Diameters were conserved with an average $D_{3,2}$ = 328 ± 68 µm before polymerization and $D_{3,2}$ = 332 ± 91 µm after polymerization attesting from the good emulsion stability during polymerization.

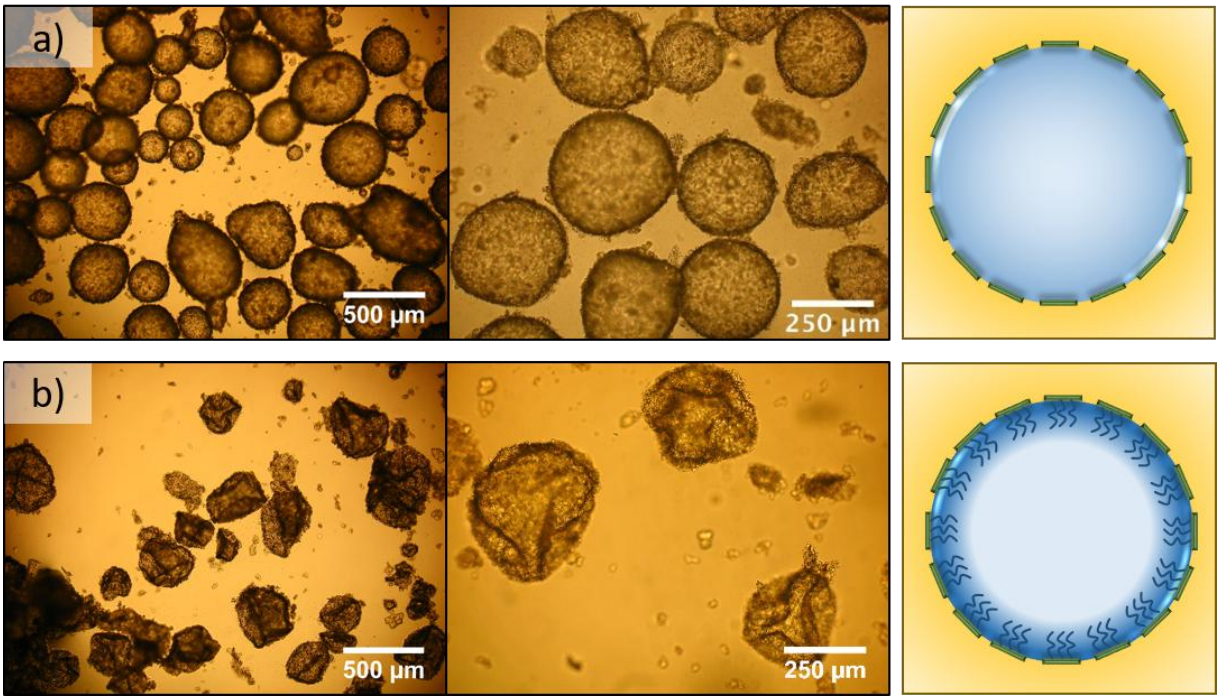

Figure 12: Optical microscopy pictures of SI-ATRP emulsion diluted in IPM a) before and b) after polymerization at different magnifications

3.4. Morphology study of polymerized emulsions

An important point to underline concerning the two polymerization processes is the different initiation locus. With free radical polymerization, polymerization occurs inside the macromonomers droplets whereas with SI-ATRP the chains grow at the CNC-shell surface. Therefore, polymer particle morphologies were expected to differ as well. From optical microscopy observation, a first difference is noticeable between emulsions polymerized by free radical polymerization and SI-ATRP (comparison between Figure 6 and Figure 12b). Indeed, emulsions polymerized by free radical polymerization kept their spherical shape even after polymerization whereas for SI-ATRP emulsions, the objects originally spherical appeared collapsed in liquid medium with a solid interface, as if folded, after polymerization. This is likely due to the loss of water by evaporation during the polymerization conducted at 50 °C. Further characterization was performed to investigate this morphological difference. Scanning electron microscopy (SEM) was used to assess the polymerized emulsions behavior in a dry state under a vacuum of 10^{-5} Pa (Figure 13). All objects indifferently from the polymerization process or formulation choices showed the presence of a dense cover of

nanoparticles at their surface. The accumulation of hydrophobic particles at the surface of the polymer particles might be responsible of the non-redispersibility of the polymerized emulsions in a hydrophilic medium.

Concerning the free radical polymerization route, samples with the lower concentration of macromonomer (10 wt%) which presented a spherical structure in dispersed medium collapsed under the SEM chamber vacuum. This behavior is likely due to its very low filling in polymer, only 70% of conversion of the 10 wt% macromonomer present in the dispersed phase. As the concentration in macromonomer increased, no deformation of the beads was induced by the vacuum anymore. Cuts of the beads were performed manually and revealed a full polymer core. Indeed, even if the macromonomer represented only a maximum of 40 wt% of the dispersed phase, the highly hydrophilic macromonomer OEGMA was able to occupy all the volume leaving no void in the polymer particle core. On the contrary, emulsions which undergone SI-ATRP displayed a hollow bead morphology with its solid shell composed of CNC-OEGMA-Br. This morphology was already observed by Zhang *et al.* who studied the formation of hollow microcapsules using CNC-stabilized Pickering emulsions as templates[10]. Polymerizing N-isopropylacrylamide (NIPAM) monomer in W/O emulsions through free radical polymerization, they were able to generate hollow microcapsules because of the insolubility of cross-linked polyNIPAM in water, therefore migrating at the droplet interface creating an inner void. The present strategy leads to a similar final morphology, for a different reason, independently of the polymer characteristics, and creates an additional covalent bonding between the polymer and the CNC shell, which could be of high interest to combine both the polymer and the stabilizing particles properties within a unique protective shell.

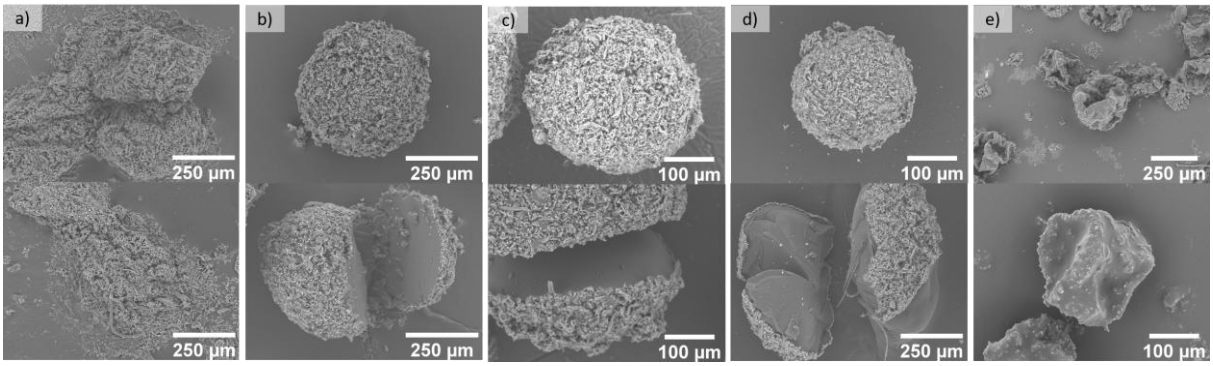

Figure 13: SEM observation of the obtained polymerized emulsion by free radical polymerization, a) 10 wt% OEGMA, b) 20 wt% OEGMA, c) 40 wt% OEGMA, d) 40 wt%(OEGMA, TEGDA 15 mol%) and by SI-ATRP e) 40 wt% OEGMA

3.5. Mechanical properties of polymerized emulsions

Full beads obtained by free radical polymerization were further investigated to assess their mechanical properties and the impact of formulation parameters like the presence of a cross-linker or the number of surrounding CNC layers. The different polymer beads were submitted to cycles of compression and relaxation using a rheometer coupled with a home-made device described in the instrumentation section. Prior to samples compression, reliability of the measurement coupling the home-made device and the rheometer was assessed by measuring compression profiles of the empty compression device, and comparing it to profiles obtained using a traction force apparatus (Fig. S13, SI). This test showed that the home-made device was rigid enough in order not to deform upon compression, and that the rheometer was adapted for the capsule compression.

3.5.1 Impact of the cross-linking

Emulsions containing OEGMA (E1, Figure 14) or both OEGMA and TEGDA (E2, Figure 14) were formulated and polymerized following the process described in section 3.2 (free radical polymerization). Their SEM observation prior to mechanical testing revealed spherical beads with a dense layer of CNCs at their surface (Figure 14 a, b, e). Polymer beads diluted in IPM were introduced in the device and submitted first to several cycles of low compression to induce the beads rearrangement by rolling and sliding[36] until a steady state was reached (Fig. S14, SI). The smoothness of the plot and the equilibrium state reached indicated the

absence of rupture and were consistent with the behavior of solid beads compared to a non-polymerized emulsion which was entirely crushed by the same test (Fig. S15, SI). Once the beads were rearranged in a stationary state, compressions of 10%, 25% and 50% of the sample were subsequently applied. The resulting stress-strain curves during compression and relaxation were plotted in Figure 15A. Different domains can be distinguished, first a linear elastic domain followed by a plastic deformation and a stiffening. Contrary to usual solids, no plateau could be observed[37], and similarities with "J-shaped" curves could be noticed, characteristic of biomaterials as soft tissues or hydrogels[38]. Another interesting feature is the absence of breakage even at high deformation (up to 40%, corresponding to 40 kPa which was the apparatus upper stress limit with the chosen geometry), and the total reversibility of the imposed strain, showing that the polymer beads behave like small sponges as it was already observed in previous work for similar systems without a particle shell[25]. This observation was further verified by SEM observation of the polymer beads after compression, which integrity was kept and no crack could be observed (Figure 14 h, i). The same observation was made when adding the cross-linker to the emulsion formulation, so that the cross-linking did not affect the sponge behavior and mechanical resistance of the polymerized emulsions.

Compression moduli were extracted from the elastic linear domains to quantify the mechanical properties of the objects (Figure 15B), showing that the addition of the cross-linker strongly reinforced the material by a factor 4.5, from 27 kPa to 124 kPa. These values are in the same order of magnitude as other organic polymer particles, which possess compression moduli ranging from a dozen of kPa to a few MPa[39–41], however comparison should be taken with care. Indeed, most studies focus on the compression of a single bead instead of assemblies as proposed here, and polymers or process can differ, using whether uniaxial compression or osmotic compression for instance. As a more direct comparison to our system, assemblies of glass beads of hundreds of micron in diameter were compressed using the same home-made device. Compression modulus of approximately 900 kPa was

measured (Fig. S13, SI), showing the great difference in behaviour with the soft deformable studied polymer beads.

3.5.2 Impact of the number of CNC layers

As it was demonstrated, the number of layer of CNC particles surrounding each droplet can be tuned by adapting the washing procedure of the CNC before freeze-drying. Therefore, 3 different batches of CNCs were prepared in order to reach different covering ratio. Emulsions E2, E3, E4 were consequently formulated with equivalent diameters stabilized by respectively 41, 15 and 6 layers of CNCs (coverage determined by Eq. 4, formulation details Fig. S3, Fig. S16, SI). SEM observation of the surface of the polymer particles clearly demonstrated the differences in coverage of the different emulsions (Figure 14 e, f, g). The surface roughness decreased with decreasing number of CNC layers, as they were also less aggregated.

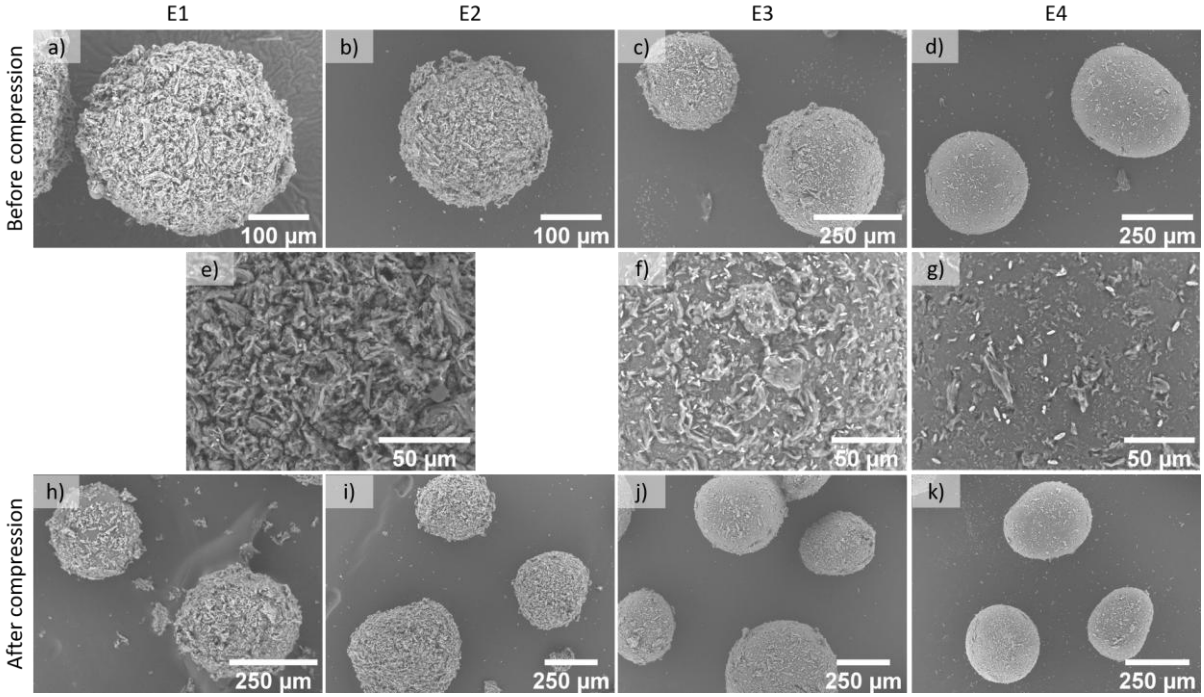

Figure 14 : Polymer particles with different macromonomer and CNC composition; a), e), h) with solely OEGMA and 41 layers of CNC; b), e), i) with OEGMA and TEGDA and 41 layers of CNC; c), f), j) with OEGMA and TEGDA and 15 layers of CNC; d) g), k) with OEGMA and TEGDA and 6 layers of CNC.

The impact of the number of CNC layers over the mechanical properties was assessed as previously, by compression. Samples E2 to E4 were submitted to several cycles of

compression-relaxation until a steady state was reached, and then compression with an applied strain of 10%, 25% and 50%. As observed for samples with E2 displaying 41 layers of CNC, no breakage nor unrecoverable deformation of the polymer particles was observed after compression (Figure 14 i, j, k, Fig. S17, SI). Whatever the number of CNC layers, the polymer particles were resistant and were able to endure up to 40% deformation. The compression moduli were extracted from the linear elastic domain and plotted in Figure 15C, showing an increase of the modulus with the number of CNC layers, from 56 kPa to 124 kPa. The difference was less noticeable between the samples E3 and E4 displaying respectively 15 and 6 layers of CNCs and moduli of 61 kPa and 56 kPa. This could be explained by a possible threshold effect, requiring a minimum amount of CNC layers to increase significantly the compression modulus of the objects, or by the fact that the difference between 15 and 6 layers is not large enough and does not induce a sensible enough modulus difference. Overall, depending on the formulation parameters, mechanical properties of the polymer particles can be tuned, from soft deformable beads using only OEGMA with a poor CNC coverage, to strong still deformable beads by the creation of a polymer network and increasing the average number of CNC covering layers.

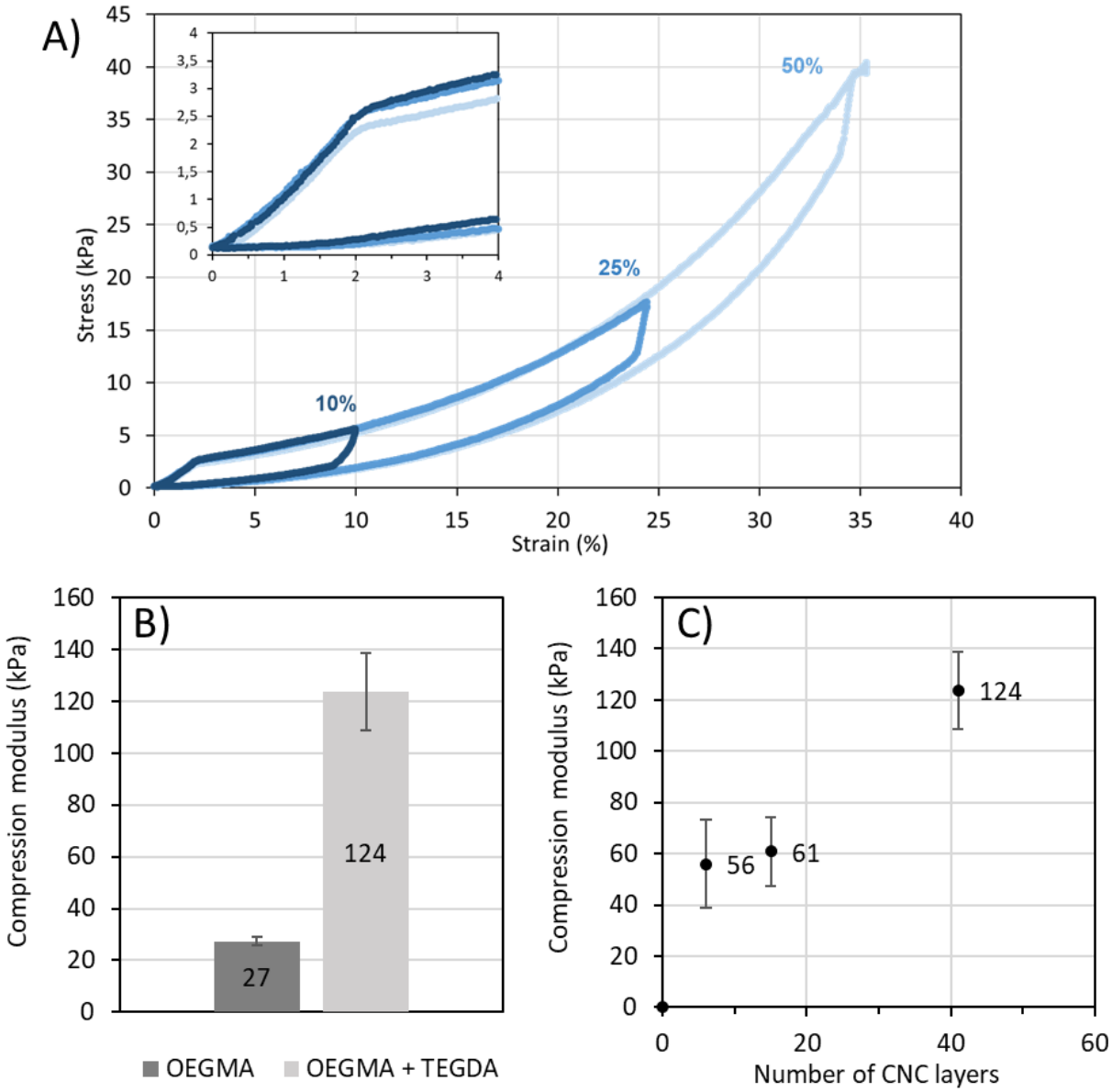

Figure 15: Mechanical properties of the polymer particles, A) stress-strain curve at different imposed compressions for E2, B) impact of the cross-linking on the compression modulus, C) impact of the number of CNC layers on the compression modulus

4. Conclusion

It has been demonstrated that brominated cellulose nanocrystals could be used as Pickering emulsion stabilizers for W/O Pickering emulsion formulation and their further polymerization. Hydroxyl oligoethylene glycol methacrylate (OEGMA, M_n = 360 g/mol) was efficiently polymerized by both free and controlled radical polymerization without destabilization, and led to two distinct polymer particle morphologies. Both polymerization routes presented interesting features as a short polymerization time of a few hours to access high conversion

rates up to 90%. Classical free radical polymerization of the hydrophilic (macro)monomer(s) enabled the formation of full beads of evenly distributed polymer which could withstand vacuum of SEM chambers, and presented a dense coverage of CNCs on their surface. These objects showed to behave as small sponges, and could be compressed up to 40% deformation without rupture and with a total recovery of their initial shape upon relaxation. High compression moduli of 27 to 124 kPa were measured, increasing with the addition of a cross-linker (TEGDA), and with the number of CNC layers. On the other hand, controlled radical polymerization led to the formation of hollow capsules, constituted of a solid shell of CNC-OEGMA-Br, by simply positioning the initiation site onto the stabilizing particles. This strategy proposes a simple way of producing polymer particles from water-soluble (macro)monomers stabilized by organic particles with natural origin and access at the same time original morphologies easily. Hence, the modification step of the CNCs is taken advantage of, by allowing both the W/O emulsion stabilization and by suggesting the future initiation site for the polymer shell. The range of objects accessible by this technique could raise interest for bio-related applications given their high stability, innocuity and mechanical similarities with soft tissues.

Supporting Information

Characterization of CNCs, ^{1}H NMR of OEGMA, Synthesis details of CNC-Br 1, CNC-Br 2A and CNC-Br 2B batches, emulsion formulation optimization details, emulsion polymerization optimization details, TGA of polymerized emulsions, swelling of OEGMA/TEGDA gels in water, reliability tests on the compression device, compression-relaxation cycles on polymerized/non-polymerized emulsions, stress-strain curves of polymerized emulsions.

Acknowledgements

HD would like to thank the French “Fondation Bordeaux Université” and the “Fonds Ernest Solvay” supported by “Fondation Roi Baudouin” for their financial support. EL, VS and VH

thank their employer CNRS and the respective academic institution of their laboratories for financial support.

References

(1) Pickering, S. U. CXCVI.—Emulsions. *J. Chem. Soc. Trans.* **1907**, *91*, 2001–2021.

(2) Ramsden, W. Separation of Solids in the Surface-Layers of Solutions and 'Suspensions' (Observations on Surface-Membranes, Bubbles, Emulsions, and Mechanical Coagulation).—Preliminary Account. *Proc. R. Soc. London* **1904**, *72 (477-48*, 156–164.

(3) Arditty, S.; Schmitt, V.; Giermanska-Kahn, J.; Leal-Calderon, F. Materials Based on Solid-Stabilized Emulsions. *J. Colloid Interface Sci.* **2004**, *275*, 659–664. https://doi.org/10.1016/j.jcis.2004.03.001.

(4) Binks, B. P. Particles as Surfactants Similarities and Differences. *Curr. Opin. Colloid Interface Sci.* **2002**, *7*, 21–41.

(5) Dupont, H.; Maingret, V.; Schmitt, V.; Héroguez, V. New Insights into the Formulation and Polymerization of Pickering Emulsions Stabilized by Natural Organic Particles. *Macromolecules* **2021**, *54* (11), 4945–4970. https://doi.org/10.1021/acs.macromol.1c00225.

(6) Habibi, Y.; Lucia, L. A.; Rojas, O. J. Cellulose Nanocrystals: Chemistry, Self-Assembly, and Applications. *Chem Rev* **2010**, *110*, 3479–3500. https://doi.org/10.1021/cr900339w.

(7) Kalashnikova, I.; Bizot, H.; Cathala, B.; Capron, I. New Pickering Emulsions Stabilized by Bacterial Cellulose Nanocrystals. *Langmuir* **2011**, *27* (12), 7471–7479. https://doi.org/10.1021/la200971f.

(8) Werner, A.; Schmitt, V.; Sèbe, G.; Héroguez, V. Convenient Synthesis of Hybrid Polymer Materials by AGET-ATRP Polymerization of Pickering Emulsions Stabilized

by Cellulose Nanocrystals Grafted with Reactive Moieties. *Biomacromolecules* **2019**, *20* (1), 490. https://doi.org/10.1021/acs.biomac.8b01482.

(9) Saelices, C. J.; Save, M.; Capron, I. Synthesis of Latex Stabilized by Unmodified Cellulose Nanocrystals: The Effect of Monomers on Particle Size. *Polym. Chem.* **2019**, *10*, 727. https://doi.org/10.1039/c8py01575a.

(10) Zhang, Z.; Cheng, M.; San Gabriel, M.; Albuquerque, Â.; Neto, T.; Da, J.; Bernardes, S.; Berry, R.; Tam, K. C. Polymeric Hollow Microcapsules (PHM) via Cellulose Nanocrystal Stabilized Pickering Emulsion Polymerization. *J. Colloid Interface Sci.* **2019**, *555*, 489–497. https://doi.org/10.1016/j.jcis.2019.07.107.

(11) Werner, A.; Sèbe, G.; Héroguez, V. A New Strategy to Elaborate Polymer Composites via Pickering Emulsion Polymerization of a Wide Range of Monomers. *Polym. Chem.* **2018**, *9*, 5043. https://doi.org/10.1039/c8py01022f.

(12) Bai, L.; Jiang, X.; Liu, B.; Wang, W.; Chen, H.; Xue, Z.; Niu, Y.; Yang, H.; Wei, D. RAFT-Mediated Pickering Emulsion Polymerization with Cellulose Nanocrystals Grafted with Random Copolymer as Stabilizer †. *RSC Adv.* **2018**, *8*, 28660. https://doi.org/10.1039/c8ra03816c.

(13) Li, H.; Zhou, J.; Zhao, J.; Li, Y.; Lu, K. Synthesis of Cellulose Nanocrystals-Armored Fluorinated Polyacrylate Latexes via Pickering Emulsion Polymerization and Their Film Properties. *Colloids Surfaces B Biointerfaces* **2020**, *192*, 111071. https://doi.org/10.1016/j.colsurfb.2020.111071.

(14) Chakrabarty, A.; Teramoto, Y. Scalable Pickering Stabilization to Design Cellulose Nanofiber-Wrapped Block Copolymer Microspheres for Thermal Energy Storage. *ACS Sustain. Chem. Eng.* **2020**, *8* (11), 4623–4632. https://doi.org/10.1021/acssuschemeng.0c00687.

(15) Zhou, J.; Wang, X.; Li, Y.; Li, H.; Lu, K. Preparation of Cellulose Nanocrystal-Dressed

Fluorinated Polyacrylate Latex Particles via RAFT-Mediated Pickering Emulsion Polymerization and Application on Fabric Finishing. *Cellulose* **2020**, *27* (11), 6617–6628. https://doi.org/10.1007/s10570-020-03227-1.

(16) Zhou, J.; Li, Y.; Li, H.; Yao, H. Cellulose Nanocrystals/Fluorinated Polyacrylate Soap-Free Emulsion Prepared via RAFT-Assisted Pickering Emulsion Polymerization. *Colloids Surfaces B Biointerfaces* **2019**, *177* (November 2018), 321–328. https://doi.org/10.1016/j.colsurfb.2019.02.005.

(17) Moreno, A.; Sipponen, M. H. Biocatalytic Nanoparticles for the Stabilization of Degassed Single Electron Transfer-Living Radical Pickering Emulsion Polymerizations. *Nat. Commun.* **2020**, *11* (1), 1–8. https://doi.org/10.1038/s41467-020-19407-3.

(18) Wang, G.; Xi, M.; Bai, L.; Liang, Y.; Yang, L.; Wang, W.; Chen, H.; Yang, H. Pickering Emulsion of Metal-Free Photoinduced Electron Transfer-ATRP Stabilized by Cellulose Nanocrystals. *Cellulose* **2019**, *26* (10), 5947–5957. https://doi.org/10.1007/s10570-019-02528-4.

(19) Nypelö, T.; Rodriguez-Abreu, C.; Kolena'ko, Y. V.; Rivas, J.; Rojas, O. J.; Kolen'ko, Y. V; Rivas, J.; Rojas, O. J.; Nypelö, T.; Rodriguez-Abreu, C.; Kolen'ko, Y. V; Josérivas, J.; Rojas, O. J. Microbeads and Hollow Microcapsules Obtained by Self-Assembly of Pickering Magneto-Responsive Cellulose Nanocrystals. *ACS Appl. Mater. Interfaces* **2014**, *6* (19), 16851–16858. https://doi.org/10.1021/am504260u.

(20) Werner, A.; Schmitt, V.; Sèbe, G.; Héroguez, V. Synthesis of Surfactant-Free Micro- and Nanolatexes from Pickering Emulsions Stabilized by Acetylated Cellulose Nanocrystals. *Polym. Chem.* **2017**, *8* (39), 6064–6072. https://doi.org/10.1039/c7py01203a.

(21) Zhai, K.; Pei, X.; Wang, C.; Deng, Y.; Tan, Y.; Bai, Y.; Zhang, B.; Xu, K.; Wang, P. Water-in-Oil Pickering Emulsion Polymerization of N-Isopropyl Acrylamide Using

Starch-Based Nanoparticles as Emulsifier. *Int. J. Biol. Macromol.* **2019**, *131*, 1032–1037. https://doi.org/10.1016/j.ijbiomac.2019.03.107.

(22) Zhai, K.; Zhang, F.; Wang, C.; Pei, X.; Tan, Y.; Bai, Y.; Zhang, B.; Wang, Y.; Xu, K.; Wang, P. Synthesis of Millimeter-sized Hydrogel Beads by Inverse Pickering Polymerization Using Starch-based Nanoparticles as Emulsifier. *Polym. Adv. Technol.* **2020**, *31* (6), 1321–1329. https://doi.org/10.1002/pat.4861.

(23) Meng, T.; Gao, X.; Zhang, J.; Yuan, J.; Zhang, Y.; He, J. Graft Copolymers Prepared by Atom Transfer Radical Polymerization (ATRP) from Cellulose. *Polymer (Guildf).* **2008**, *50*, 447–454. https://doi.org/10.1016/j.polymer.2008.11.011.

(24) Morandi, G.; Heath, L.; Thielemans, W. Cellulose Nanocrystals Grafted with Polystyrene Chains through Surface Initiated Atom Transfer Radical Polymerization (SI-ATRP). *Langmuir* **2009**, *25* (14), 5. https://doi.org/10.1021/la900452a.

(25) Stasse, M.; Laurichesse, E.; Vandroux, M.; Ribaut, T.; Héroguez, V.; Schmitt, V. Cross-Linking of Double Oil-in-Water-in-Oil Emulsions: A New Way for Fragrance Encapsulation with Tunable Sustained Release. *Colloids Surfaces A Physicochem. Eng. Asp.* **2020**, *607*, 125448. https://doi.org/10.1016/j.colsurfa.2020.125448.

(26) Dupont, H.; Fouché, C.; Dourges, M.-A.; Schmitt, V.; Héroguez, V. Polymerization of Cellulose Nanocrystals-Based Pickering HIPE towards Green Porous Materials. *Carbohydr. Polym.* **2020**, *243*, 116411. https://doi.org/10.1016/j.carbpol.2020.116411.

(27) Saidane, D.; Perrin, E.; Cherhal, F.; Guellec, F.; Capron, I. Some Modification of Cellulose Nanocrystals for Functional Pickering Emulsions. *Phil. Trans. R. Soc. A* **2016**, *374*, : 20150139. https://doi.org/10.1098/rsta.2015.0139.

(28) Hu, Z.; Ballinger, S.; Pelton, R.; Cranston, E. D. Surfactant-Enhanced Cellulose Nanocrystal Pickering Emulsions. *J. Colloid Interface Sci.* **2015**, *439*, 139–148. https://doi.org/10.1016/j.jcis.2014.10.034.

(29) Peddireddy, K. R.; Nicolai, T.; Benyahia, L.; Capron, I. Stabilization of Water-in-Water Emulsions by Nanorods. *ACS Macro Lett.* **2016**, *5*, 283–286. https://doi.org/10.1021/acsmacrolett.5b00953.

(30) Arditty, S.; Whitby, C. P.; Binks, B. P.; Schmitt, V.; Leal-Calderon, F. Some General Features of Limited Coalescence in Solid-Stabilized Emulsions. *Eur. Phys. J. E* **2003**, *11*, 273–281. https://doi.org/10.1140/epje/i2003-10018-6.

(31) Wiley, R. M. Limited Coalescence of Oil Droplets in Coarse Oil-in-Water Emulsions. *J. Colloid Sci.* **1954**, *9* (5), 427–437. https://doi.org/10.1016/0095-8522(54)90030-6.

(32) Schmitt, V.; Destribats, M.; Backov, R. Colloidal Particles as Liquid Dispersion Stabilizer: Pickering Emulsions and Materials Thereof. *Comptes Rendus Phys.* **2014**, *15* (8–9), 761–774. https://doi.org/10.1016/j.crhy.2014.09.010.

(33) Buback, M.; Feldermann, A.; Barner-Kowollik, C.; Lacík, I. Propagation Rate Coefficients of Acrylate-Methacrylate Free-Radical Bulk Copolymerizations. *Macromolecules* **2001**, *34*, 5439–5448. https://doi.org/10.1021/ma002231w.

(34) Stasse, M.; Ribaut, T.; Schmitt, V.; Héroguez, V. Encapsulation of Lipophilic Fragrance by Polymerization of the Intermediate Aqueous Phase of an Oil-in-Water-in-Oil (O/W/O) Double Emulsion. *Polym. Chem.* **2019**, *10* (30), 4154–4162. https://doi.org/10.1039/C9PY00528E.

(35) Siegwart, D. J.; Oh, J. K.; Gao, H.; Bencherif, S. A.; Perineau, F.; Bohaty, A. K.; Hollinger, J. O.; Matyjaszewski, K. Biotin-, Pyrene-, and GRGDS-Functionalized Polymers and Nanogels via ATRP and End Group Modification. *Macromol. Chem. Phys.* **2008**, *209* (21), 2179–2193. https://doi.org/10.1002/macp.200800337.

(36) Brzesowsky, R. H.; Spiers, C. J.; Peach, C. J.; Hangx, S. J. T. Time-Independent Compaction Behavior of Quartz Sands. *J. Geophys. Res. Solid Earth* **2014**, *119*, 936–956. https://doi.org/10.1002/ 2013JB010444.

(37) Maiti, S. K.; Gibson, L. J.; Ashby, M. F. Deformation and Energy Absorption Diagrams for Cellular Solids. *Acta Metall.* **1984**, *32* (11), 1963–1975. https://doi.org/10.1016/0001-6160(84)90177-9.

(38) Holzapfel, G. A. Biomechanics of Soft Tissue. *Handb. Mater. Behav. Model.* **2000**, *3*, 1049–1063.

(39) Egholm, R. D.; Christensen, S. F.; Szabo, P. Stress-Strain Behavior in Uniaxial Compression of Polymer Gel Beads. *J. Appl. Polym. Sci.* **2006**, *102* (3), 3037–3047. https://doi.org/10.1002/app.24715.

(40) Kaygusuz, H.; Güls¸, G.; Akın Evingür, G.; Pekcan, Ö.; Von Klitzing, R.; Bedia Erim, F. Surfactant and Metal Ion Effects on the Mechanical Properties of Alginate Hydrogels. *Int. J. Biol. Macromol.* **2016**, *92*, 220–224. https://doi.org/10.1016/j.ijbiomac.2016.07.004.

(41) Dolega, M. E.; Delarue, M.; Ingremeau, F.; Prost, J.; Delon, A.; Cappello, & G. Cell-like Pressure Sensors Reveal Increase of Mechanical Stress towards the Core of Multicellular Spheroids under Compression. *Nat. Commun.* **2017**, *8*, 14056. https://doi.org/10.1038/ncomms14056.

For Table of Content (ToC) only